Nano Research 2016, 9(2): 458–472
DOI 10.1007/s12274-015-0928-2
Research Article
ISSN 1998-0124
CN 11-5974/O4

Multi-walled carbon nanotubes covalently functionalized by axially coordinated metal-porphyrins: Facile syntheses and temporally dependent optical performance

Aijian Wang[1,2,3], Jingbao Song[1], Zhipeng Huang[1], Yinglin Song[4], Wang Yu[1], Huanli Dong[5], Wenping Hu[5], Marie P. Cifuentes[6], Mark G. Humphrey[6], Long Zhang[3], Jianda Shao[3], and Chi Zhang[2,3,6] (✉)

[1] *China-Australia Joint Research Center for Functional Molecular Materials, Scientific Research Academy, Jiangsu University, Zhenjiang 212013, China*
[2] *China-Australia Joint Research Center for Functional Molecular Materials, School of Chemical and Material Engineering, Jiangnan University, Wuxi 214122, China*
[3] *Key Laboratory of Materials for High-Power Laser, Shanghai Institute of Optics and Fine Mechanics, Chinese Academy of Sciences, Shanghai 201800, China*
[4] *School of Physical Science and Technology, Soochow University, Suzhou 215006, China*
[5] *Key Laboratory of Organic Solids, Institute of Chemistry, Chinese Academy of Sciences, Beijing 100190, China*
[6] *Research School of Chemistry, Australian National University, Canberra, ACT 2601, Australia*

Received: 5 June 2015
Revised: 25 October 2015
Accepted: 26 October 2015

KEYWORDS
metal-porphyrin,
axially coordinated,
multi-walled carbon nanotubes,
facile syntheses,
optical performance,
cycloaddition

ABSTRACT

Axially coordinated metal-porphyrin-functionalized multi-walled carbon nanotube (MWCNT) nanohybrids were prepared via two different synthetic approaches (a one-pot 1,3-dipolar cycloaddition reaction and a stepwise approach that involved 1,3-dipolar cycloaddition followed by nucleophilic substitution), and characterized through spectroscopic techniques. Attachment of the tin porphyrins to the surface of the MWCNTs significantly improves their solubility and ease of processing. These axially coordinated (5,10,15,20-tetraphenylporphyrinato)tin(IV) (SnTPP)-MWCNTs exhibit significant fluorescence quenching. The third-order nonlinear optical properties of the resultant nanohybrids were studied by using the Z-scan technique at 532 nm with both nanosecond and picosecond laser pulses. The results show that the nanohybrids exhibit significant reverse saturable absorption or saturable absorption when nanosecond or picosecond pulses, respectively, are employed. Improvement in the nanosecond regime nonlinear absorption is observed on proceeding to the nanohybrids and is ascribed to a combination of the outstanding properties of MWCNTs and the chemically attached metal-porphyrins.

1 Introduction

Nanostructures are poised to be the future building blocks for electronic and photonic devices [1–3], a prospect that has spurred widespread research into such materials, particularly those exhibiting important

Address correspondence to chizhang@jiangnan.edu.cn, czhang@siom.ac.cn, chi.zhang@anu.edu.au

nonlinear optical (NLO) properties (including optical limiting) that can be used to protect optical sensors (human eyes or highly sensitive charge-coupled device (CCD) cameras) from damage caused by intense laser pulses [4–6]. Interestingly, several nanohybrids have been shown to possess improved optical nonlinearities compared to their bulk counterparts [7–10]. Design and synthesis of novel nanomaterials with the required NLO functions for practical limiters, however, still present a significant challenge. Recent studies have shown that multi-walled carbon nanotubes (MWCNTs) and related nanomaterials have superior NLO performances to traditional conjugated organic molecules because of their more extensive π-conjugated networks (and thereby, their abundance of π-electrons) [11–13]. However, the application of MWCNTs has been impeded by difficulties associated with processing and manipulation, owing to their extremely poor solubility that is a result of substantial van der Waals attractions between MWCNTs along their long axis [14, 15]. Thus, considerable effort has been devoted toward the covalent or non-covalent functionalization of MWCNTs by organic NLO-chromophores in order to simultaneously promote the solubility and the NLO function of suspensions of the MWCNTs. Indeed, an additional limiting effect was observed for organic NLO-chromophore-functionalized MWCNTs at some wavelengths, owing to dye photo-induced electron and/or energy transfer to the MWCNTs [16, 17]; optical nonlinearities of nanohybrids can therefore be optimized upon electronic photo-activation of the partners.

Among these organic nonlinear chromophores, porphyrins are known to possess unique characteristics (the optical properties can be modulated by changing the type of axial ligands, the central metal, and the nature of the substituents at the macrocyclic periphery) that render them superior to other compounds as photoactive materials [18], and that can be used in the design of efficient NLO materials. The architectural flexibility inherent in porphyrins, such as the ability to append electron-acceptor subunits to the central metal atom and thereby introduce a dipole moment perpendicular to the macrocycle in the axially substituted porphyrins, provides additional ways to optimize the NLO response [9]. Some carbon-nanotube- and porphyrin-based hybrids have been reported that possess excellent optoelectronic effects [13, 16, 19, 20]; however, to the best of our knowledge, there have been no reports thus far of axially functionalized MWCNT-porphyrin nanohybrids, which might provide more efficient electron transferability to the entire nanostructure.

Herein, we report the preparation of MWCNT hybrid materials incorporating axially functionalized porphyrins through two synthetic routes: A straightforward Prato reaction (i.e., 1,3-dipolar cycloaddition reaction) with sarcosine and a formyl-containing porphyrin, and a stepwise method at a minimal synthetic cost that involves a 1,3-dipolar cycloaddition to the MWCNT surface using 4-hydroxybenzaldehyde followed by nucleophilic substitution with an appropriate porphyrin. Indeed, the latter can be considered to be the optimized synthesis of MWCNT-di(4-formylphenoxy)(5,10,15,20-tetraphe-nylporphyrinato)tin(IV) (SnTPP **1**) that affords the similar nanohybrid system MWCNT-dichloro(5,10,15,20-tetraphenylporphyrinato)tin(IV) (SnTPP **2**). The nanohybrids thus prepared are stable in polar solvents such as dimethylformamide (DMF) and dimethylsulfoxide (DMSO), forming gray-green suspensions. The differences and similarities between MWCNT-SnTPP **1** and MWCNT-SnTPP **2** were identified using a number of spectroscopic and microscopy techniques. The ground- and excited-state MWCNT-porphyrin interactions and the NLO responses of the resultant MWCNT-porphyrin nanohybrids were probed. The two nanohybrids were found to exhibit contrasting third-order NLO absorptive performances under different temporal laser pulses, while clear differences in their nonlinear optical responses were observed, highlighting the influence on photophysical properties of the degree of functionalization and the synthetic approach employed.

2 Results and discussion

2.1 Syntheses

The surface modification of MWCNTs is an important tool for their efficient combination with other materials, and has opened new avenues for fabrication of novel nanomaterials by improving solubility and processability [21]. In addition, MWCNTs are extended molecular wires, so injection of energy/electrons into

MWCNTs may result in high charge mobility [22]. MWCNTs are expected to play an important role in photo-induced energy/electron transfer, with applications in photonics and photovoltaics. The 1,3-dipolar cycloaddition of azomethine ylides onto MWCNTs may pave a new way toward this direction [23]. Using this chemistry, a large number of functional materials can be introduced onto the MWCNTs' surfaces.

"Axial-bonding" at porphyrins may provide an effective method for the preparation of arrays with tunable electrochemical and photo-responsive properties by changing the π-orbital interactions [9]. Axial substituents in porphyrins can in principle favorably influence the NLO properties because of the presence of a dipole moment that is perpendicular to the macrocycle in the axially functionalized porphyrins. However, to the best of our knowledge, there have been no reports thus far of axially functionalized MWCNT-porphyrin nanohybrids, although such constructs might result in an increase in various excited-state processes including enhanced internal conversion and intersystem crossing, excitation energy transfer, and photo-induced electron transfer. The covalent linking of an electron donor, i.e., axially coordinated tin porphyrins, has therefore been pursued in the present studies for the aforementioned aims and to improve the solubilization and broaden the utilization of MWCNTs. The trans axial ligands at Sn(IV) result in tin porphyrins with very stable six-coordinate environments. Two possible routes to functionalizing MWCNTs with axially coordinated porphyrins were considered (Scheme 1), both using 1,3-dipolar cycloaddition. The first route involved the preparation of a formyl-containing porphyrin, SnTPP **1**. The advantage of this method is that a formyl-containing porphyrin can be readily attached to MWCNTs through the formation of the corresponding azomethine ylide. A drawback of this route lies in the fact that the pristine porphyrin, SnTPP **1**, is very difficult to synthesize and purify. Consequently, we explored another method that involved an initial reaction of sarcosine and 4-hydroxybenzaldehyde with the MWCNTs, and then a subsequent nucleophilic substitution reaction of the derivatized nanotube material with SnTPP **2** (Scheme 1), which can be considered to be the optimized synthesis of MWCNT-SnTPP **1** that affords the similar nanohybrid system MWCNT-SnTPP **2**. This strategy is advantageous, as chemical modifications of carbon nanotubes usually require a large excess of the reactants [23, 24]. In the present case, 4-hydroxybenzaldehyde is inexpensive. Another important consideration is that hydroxyl

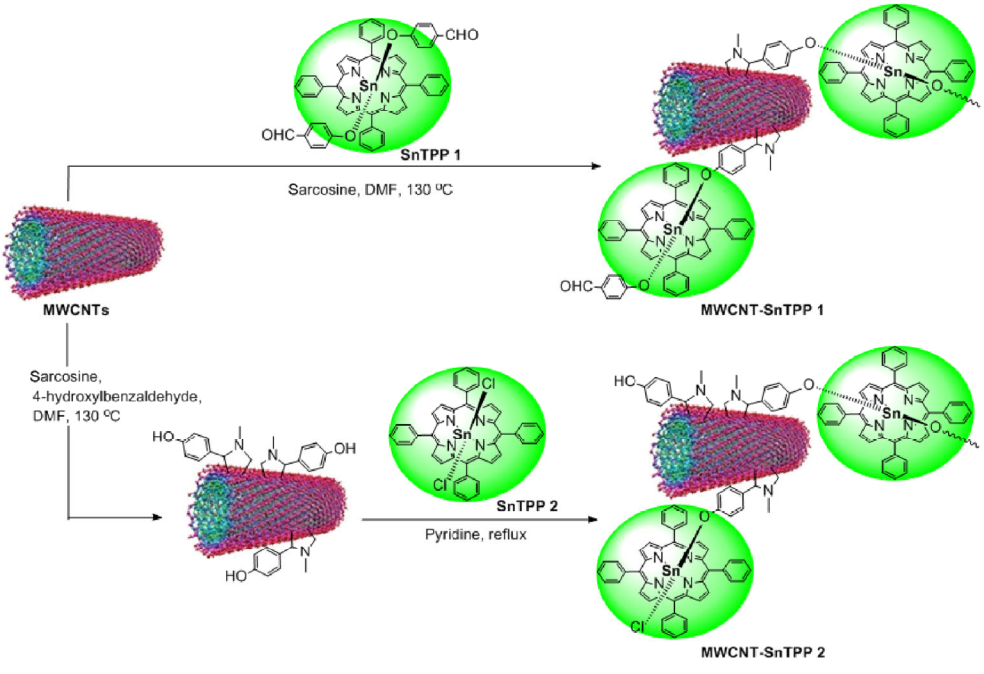

Scheme 1 Preparation of MWCNT-SnTPP **1** and MWCNT-SnTPP **2**.

groups can be grafted onto the MWCNTs' surfaces through a single reaction without degrading the MWCNTs' electronic properties, permitting a high grafting density of organic units and, potentially, wider application as an optoelectronic nanohybrid material [25]. The nucleophilic substitution of SnTPP **2** by the functionalized MWCNTs bearing pendent OH groups then proceeds under nearly stoichiometric conditions. All samples except the MWCNTs displayed very good dispersibility in DMSO, with the chemically modified MWCNT-SnTPP **1** and MWCNT-SnTPP **2** nanohybrids' dispersions having a light gray-green color (Fig. 1), consistent with the presence of the porphyrin moieties; this confirmed that attachment of the porphyrin moieties to the surface of the MWCNTs significantly improved their solubility and ease of processing. Physically adsorbed porphyrin molecules can be efficiently removed from the products by filtration and washing, as described in the Experimental section; the control experiment, in which MWCNTs were mixed with porphyrins in DMF followed by efficient filtration and washing, proved that the adsorbed porphyrin content of the nanohybrids was negligible. Therefore, the synthetic approaches presented here promise grafting of porphyrin units onto MWCNTs' surfaces with some control of extent. The covalent grafting efficiency and capacity of both methods are clearly of interest, but have rarely been evaluated previously [24]. Both **1** and **2** have been characterized through various analytical and spectroscopic techniques; all results were in agreement with successful functionalization of the MWCNTs with porphyrins.

Figure 1 Photographic images of the samples dispersed in DMSO (from left to right: MWCNTs, SnTPP **1**, MWCNT-SnTPP **1**, SnTPP **2**, and MWCNT-SnTPP **2**).

2.2 Fourier transform infrared (FTIR) spectroscopy

FTIR spectra provided evidence that covalent functionalization at the surface of the MWCNTs had been successful. Figure 2 displays the FTIR spectra for the pristine samples (MWCNTs, SnTPP **1**, and SnTPP **2**) and for the porphyrin-functionalized samples MWCNT-SnTPP **1** and MWCNT-SnTPP **2**. In the spectrum of the MWCNTs, a wide band centered at 3,450 cm^{-1} is ascribed to the presence of O–H groups on the surface of the as-received MWCNTs, resulting from atmospheric moisture tightly bound to the MWCNTs. The weak peaks in the range 2,880–2,900 cm^{-1} are consistent with the presence of $–CH_n$ species [26, 27]. The band at 1,683 cm^{-1} is assigned to the stretching of the carbon nanotube backbone. As expected, the characteristic stretching vibration of the aldehyde groups in the FTIR spectrum of SnTPP **1**, centered at 1,698 cm^{-1}, becomes much weaker in the FTIR spectrum of MWCNT-SnTPP **1**, which indicates that most of the aldehyde units had reacted but that residual aldehyde groups remained. This observation is plausible for MWCNT-SnTPP **1** according to Scheme 1, as some of the aldehyde units in SnTPP **1** may not react with the MWCNTs, consistent with the results of X-ray photoelectron spectroscopy (XPS) (Fig. S1 in the Electronic Supplementary Material (ESM)). The bands at 1,256 and 1,197 cm^{-1} correspond to the stretching vibrations of the pyrrolic C–N units. A series of strong absorption bands from 1,410 to 1,655 cm^{-1} can be ascribed to the

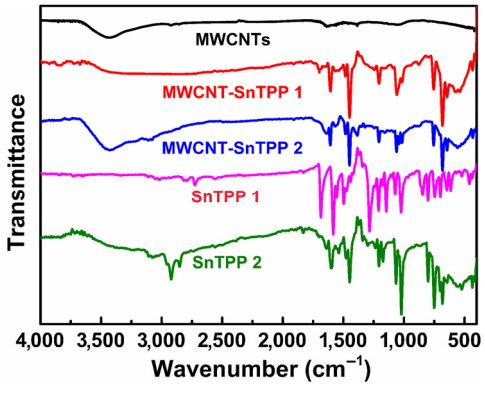

Figure 2 FTIR spectra of the MWCNTs, MWCNT-SnTPP **1**, MWCNT-SnTPP **2**, SnTPP **1**, and SnTPP **2**.

stretching vibrations of the phenyl C=C bonds of the porphyrin, and the bands observed at 660–900 cm^{-1} correspond to the out-of-plane bending vibrations of the phenyl C–H units. These bands in the FTIR spectrum of MWCNT-SnTPP **1** were consistent with those displayed by SnTPP **1**. The FTIR spectrum of MWCNT-SnTPP **2** displayed some bands that were observed in SnTPP **2**, and that were similar to those of MWCNT-SnTPP **1**. The FTIR spectral data of these two MWCNT-SnTPP nanohybrids were consistent with porphyrin moieties being grafted onto the surface of the MWCNTs. Functionalization occurs at the tip and on the outer shell of the nanotubes, rendering them easily dispersible in organic solvents.

2.3 Linear optical properties

The ultraviolet (UV)-vis spectra (Fig. 3) revealed that the MWCNTs exhibited a broad absorption maximum at 266 nm with continuously decreasing intensity over the entire UV-vis range, whilst SnTPP **1** and SnTPP **2** showed a strong Soret absorption around 422 nm and weak Q bands between 500 and 700 nm. Similar to single-walled carbon nanotube (SWCNT)-TPP ensembles [28], the overall appearances of the spectra of both MWCNT-SnTPP nanohybrids displayed the key features of those of the constituent porphyrins, with practically no shift or broadening in the Soret or Q bands (Fig. 3). The presence of MWCNTs was substantiated by the appearance of broadband absorption, as observed in the spectrum of MWCNTs. The surface of the MWCNTs may have been covered by porphyrin moieties, and this could have been the reason the features in the UV-vis absorption spectra (the position of the Soret band) of the MWCNT-SnTPP hybrids were not very different from those in the spectra of SnTPP **1** and SnTPP **2** [28, 29]. However, it is worth noting that the overall intensity of the Soret bands of the porphyrin moieties in both MWCNT-SnTPP nanohybrids was lower than those in the absorption spectra of SnTPP **1** and SnTPP **2**, and the intensity increased in proceeding from MWCNT-SnTPP **1** to MWCNT-SnTPP **2**. This implies that the porphyrin content in the MWCNT-SnTPP nanohybrids increased from MWCNT-SnTPP **1** to MWCNT-SnTPP **2** owing to the different functionalization approaches. Indeed, similar outcomes were observed in the ground-state absorption spectra of phthalocyanine-functionalized SWCNTs, corresponding to the different degrees of functionalization [13].

Fluorescence spectra of SnTPP **1** and SnTPP **2** and both MWCNT-SnTPP nanohybrids as suspensions were obtained to investigate the π–π interactions between the MWCNTs and the porphyrins (Fig. 4) (for comparative purposes, the fluorescence spectrum of the MWCNTs is also provided (Fig. S2 in the ESM)). Upon excitation of SnTPP **1**, SnTPP **2**, MWCNT-SnTPP **1**, and MWCNT-SnTPP **2** at 420 nm, and with the absorbance of the porphyrin adjusted to be identical, the fluorescence emission from the SnTPP moieties on the MWCNTs of the MWCNT-SnTPP nanohybrids was quenched strongly relative to those of SnTPP **1** and SnTPP **2**, which may be ascribed to photo-induced electron/energy transfer between SnTPP and the MWCNTs. The direct attachment of the SnTPP units to the π-conjugated surface of the MWCNTs may also facilitate quenching of the porphyrin excited singlet

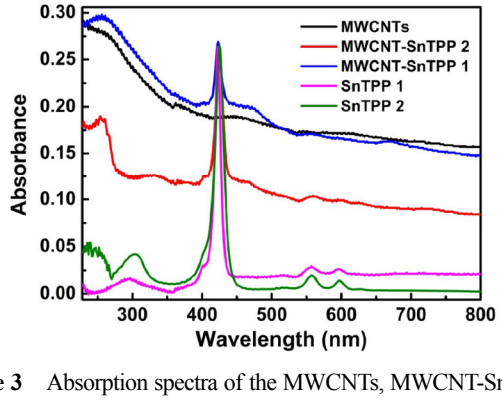

Figure 3 Absorption spectra of the MWCNTs, MWCNT-SnTPP **1**, MWCNT-SnTPP **2**, SnTPP **1**, and SnTPP **2**.

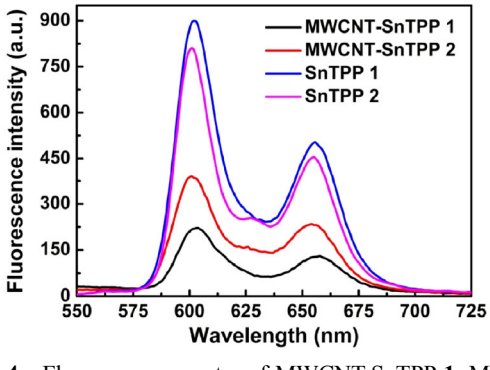

Figure 4 Fluorescence spectra of MWCNT-SnTPP **1**, MWCNT-SnTPP **2**, SnTPP **1**, and SnTPP **2** in DMSO with equivalent absorption at an excitation wavelength of 420 nm.

state in the covalently linked porphyrin-MWCNT hybrid. Electron/energy transfer quenching is known in porphyrins linked with carbon nanostructures, either covalently or by strong π–π stacking interactions [20, 30–32]. Interactions between porphyrins and carbon nanostructures invariably result in the quenching of the porphyrin fluorescence emission, via transfer of excited singlet-state energy to the carbon nanostructure, and are consistent with observations in covalent and non-covalent phthalocyanine-carbon nanostructure systems [33]. Differences in fluorescence emission were observed upon comparing MWCNT-SnTPP **1** with MWCNT-SnTPP **2**; MWCNT-SnTPP **1** exhibited 76% quenching of fluorescence emission at 604 and 657 nm, while approximately 57% fluorescence quenching was observed for MWCNT-SnTPP **2** at 601 and 654 nm, corresponding to a blue shift of 3 nm when compared to MWCNT-SnTPP **1**. Overall, the results from the absorption and fluorescence spectra measurements suggest that different reaction conditions may result in different photophysical properties and grafted porphyrin content in the MWCNT-SnTPP nanohybrids.

2.4 Raman spectroscopy

The functionalization was further evidenced by Raman spectroscopy (Fig. 5). The Raman spectra of MWCNT-based systems give rise to two principal spectral bands of interest, namely the D and G bands. The D band corresponds to defects in the disorder-induced modes (or sp^3-hybridized carbons) and is typically observed at a Raman shift of 1,343 cm^{-1}, while the G band corresponds to in-plane vibrations of the graphite wall (sp^2-hybridized carbons) [34], and is typically found at a Raman shift of 1,574 cm^{-1}. A comparison between the observed D and G bands of pristine and SnTPP-functionalized MWCNTs (MWCNT-SnTPP **1** and MWCNT-SnTPP **2**) is given in Table 1; a shift to lower frequency was observed for both nanohybrids compared to pristine MWCNTs. Similar to graphene [35], the G band of carbon nanotubes in the Raman spectrum is known to shift to higher frequencies upon conjugation with electron-acceptor components or to lower frequencies when hybridized with electron-donor moieties [36–38]. In the present case, the shifts to lower frequencies (softening) for both the D and G bands in our MWCNT-SnTPP systems in comparison

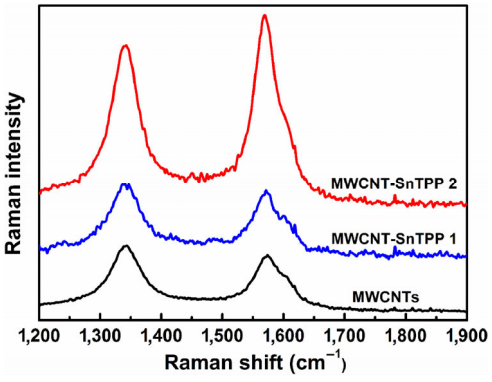

Figure 5 Raman spectra of pristine MWCNTs, MWCNT-SnTPP **1**, and MWCNT-SnTPP **2**.

Table 1 Raman spectral data obtained for the MWCNTs before and after modification with SnTPP

Samples	Frequency (cm^{-1})		I_D/I_G
	D band	G band	
MWCNTs	1,343	1,574	1.13
MWCNT-SnTPP 1	1,342	1,569	0.90
MWCNT-SnTPP 2	1,340	1,571	1.03

with those of pristine MWCNTs confirmed the occurrence of charge transfer between SnTPP and MWCNTs, where SnTPP and MWCNT units work as electron-donor and electron-acceptor components, respectively. The intensity ratio of the D band to that of the G band (I_D/I_G) indicates the extent of modification of the surface structure of the MWCNTs [12]. The I_D/I_G ratio decreased from 1.13 for MWCNTs to 0.90 for MWCNT-SnTPP **1** and 1.03 for MWCNT-SnTPP **2**. The decrease in the I_D/I_G ratio can be explained by the fact that although some sp^2 carbon atoms in the MWCNTs were transformed to sp^3 carbon atoms, the amount of sp^3 carbon atoms was still less than that of sp^2 carbon atoms in the grafted porphyrin moieties (see the structure of SnTPP). In other words, the characteristic absorption peaks of the MWCNTs can be modulated by the introduction of porphyrins through the different functionalization approaches. Since Raman scattering is strongly sensitive to the electronic structure, these results are evidence for the chemical functionalization [39].

2.5 Morphology characterization

Indirect evidence for the interactions between MWCNTs

and SnTPP can be obtained from transmission electron microscopy (TEM) (Fig. 6). The TEM specimens were obtained via the application of a few drops of the solutions of the samples in methanol onto carbon-coated copper grids and then subsequent evaporation of the solvent. As shown in Fig. 6(a), the wall surface of the pristine MWCNTs is smooth, and the hollow structure can be clearly distinguished, without detectable amorphous layers. After modification with porphyrins, the MWCNTs' surfaces became clearly rougher, while the intrinsic quality of the nanotube structures was maintained, and new species, corresponding to porphyrin molecules, could be observed (Figs. 6(b) and 6(c)). Because the SnTPP molecules that were physically bound to the MWCNT surface were removed in the purification steps, the observed morphology can be correlated to the effect of the covalent bonding between the MWCNTs and SnTPP. As shown in Figs. 6(d) and 6(e), the formation of a small number of H-shaped junctions was presumably a consequence of the connection of two MWCNTs in a "side-to-side" configuration with a SnTPP [40]. Indeed, "side-to-side" cross-linking is plausible in the present case, according to Scheme 1. The grafted porphyrin moieties may act as a surfactant, interfering with the π–π interactions between the MWCNTs, resulting in weaker nanotube interactions and thereby the debundling and solubilization of the MWCNTs [41]. The unique TEM results suggest that the reaction conditions applied in this work are indeed effective in functionalizing MWCNTs and, specifically, in the preparation of MWCNT-SnTPP nanohybrids.

2.6 Thermal properties

Investigation of the thermal degradation of materials is of significant importance owing to the fact that it can, in many cases, determine the upper temperature limit for the use of a material, while considerable attention has been directed toward exploitation of thermogravimetric data for the determination of functional groups [42]. For these reasons, and because of its simplicity and the information afforded by a simple thermogram, thermogravimetric analysis (TGA) is a widely used technique. Figure 7 shows the TGA results for the carbon nanotube materials, namely, MWCNTs, MWCNT-SnTPP **1**, and MWCNT-SnTPP **2**. As evident from the trace, MWCNTs are stable in the temperature range 50–800 ˚C. However, different thermal properties were observed for both nanohybrids, indicating the significant influence of the different synthetic routes. MWCNT-SnTPP **1** lost 43% of its weight from 50 to 800 ˚C, whereas MWCNT-SnTPP **2** underwent a mass loss of 49%. Furthermore, the thermal stability decreased as the porphyrin content increased, in proceeding from nanohybrid MWCNT-SnTPP **1** to MWCNT-SnTPP **2**.

2.7 X-ray photoelectron spectroscopy

The aim of the XPS analysis was to evaluate the

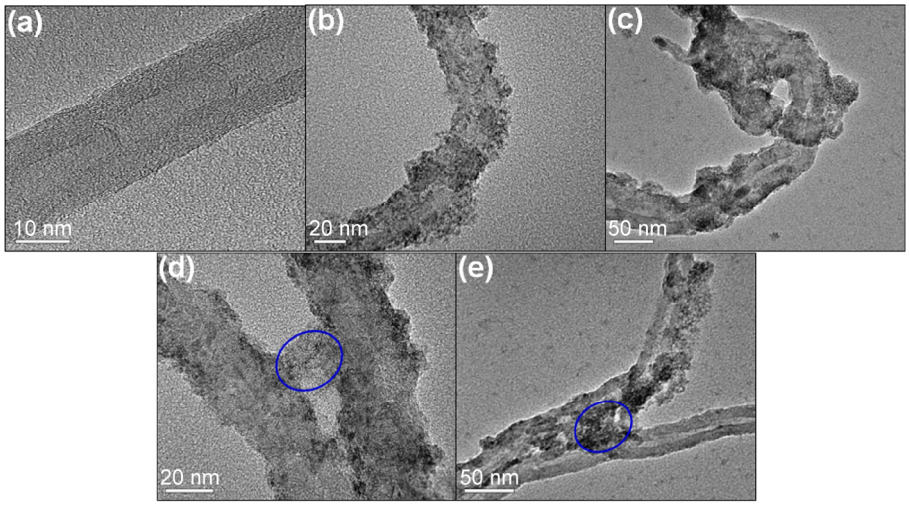

Figure 6 TEM images of (a) pristine MWCNTs, (b) and (d) MWCNT-SnTPP **1**, and (c) and (e) MWCNT-SnTPP **2**.

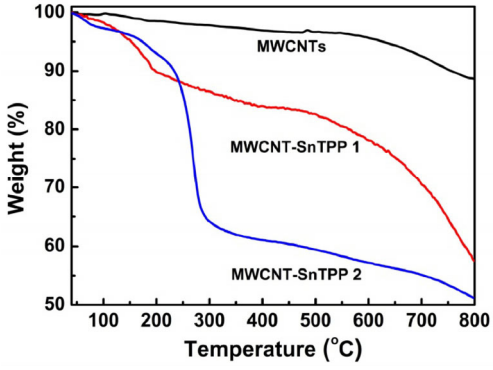

Figure 7 TGA thermograms of pristine MWCNTs, MWCNT-SnTPP **1**, and MWCNT-SnTPP **2** at a heating rate of 10 °C·min^{-1} under N_2.

elemental composition and functionality of the MWCNTs before and after modification, thereby providing a better understanding of the surface chemistries that are directly correlated to their electrical properties; the results are shown in Fig. 8. The three samples (pristine MWCNTs, MWCNT-SnTPP **1**, and MWCNT-SnTPP **2**) displayed sharp carbon peaks and weak oxygen peaks. However, compared to pristine MWCNTs (Fig. 8(a)), the oxygen peaks of MWCNT-SnTPP **1** and MWCNT-SnTPP **2** were stronger, and three new peaks related to Sn $3d_{3/2}$, Sn $3d_{5/2}$, and N 1s were observed, consistent with the successful grafting of porphyrins onto the MWCNTs. To investigate the bonding state, the high-resolution C 1s XPS spectra of MWCNT-SnTPP **1**, MWCNT-SnTPP **2**, and MWCNTs were studied. Following deconvolution, the C 1s spectrum of the MWCNTs (Fig. 8(b)) displayed four pronounced peaks at 284.1, 284.6, 285.9, and 290.6 eV corresponding to the sp^2 carbon atoms, the defects on the nanotube structure, the –C=O groups, and the π–π^* transition loss peak, respectively [43, 44]. After introduction of SnTPP, some new contributions arising from the porphyrin macrocycle could be observed in the spectra of MWCNT-SnTPP **1** and MWCNT-SnTPP **2** (Figs. 8(c) and 8(d)). The binding energies of C–O–Sn in the O 1s spectrum were 531.2 and 530.5 eV for MWCNT-SnTPP **1** and MWCNT-SnTPP **2**, respectively (Fig. S1 in the ESM). The presence of residual aldehyde groups in MWCNT-SnTPP **1** was further confirmed by the O 1s core-level XPS spectrum (Fig. S1 in the ESM), which was consistent with the FTIR analysis (Fig. 2). From the foregoing analysis, it can be concluded

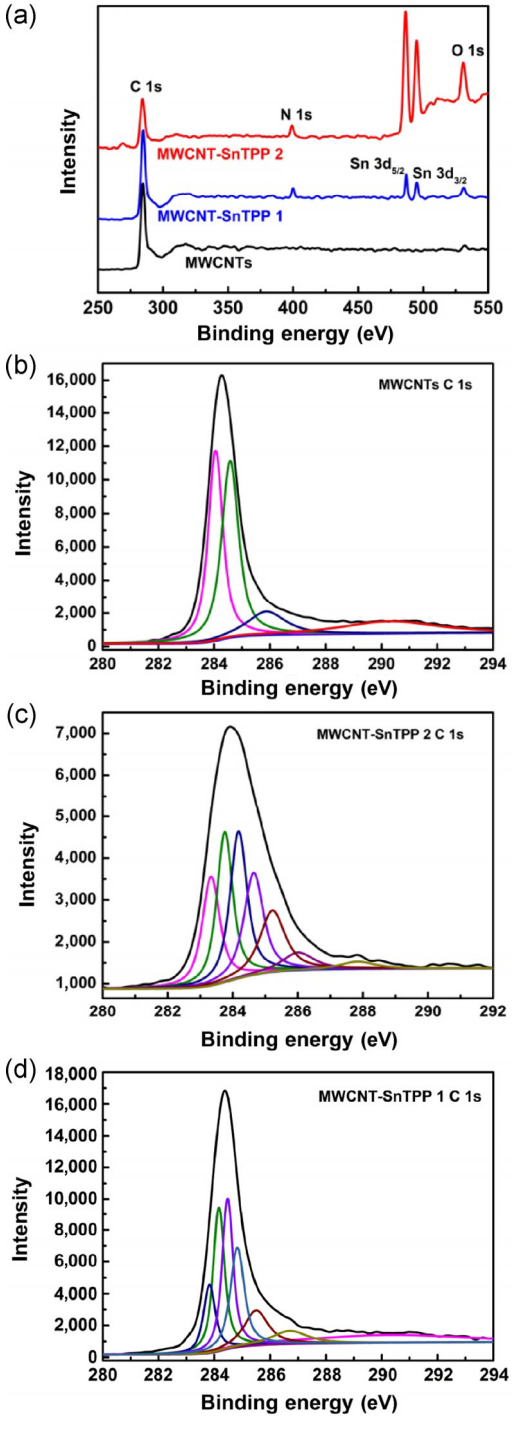

Figure 8 (a) XPS survey scans of MWCNTs, MWCNT-SnTPP **1**, and MWCNT-SnTPP **2**, and C 1s XPS spectra of (b) MWCNTs, (c) MWCNT-SnTPP **2**, and (d) MWCNT-SnTPP **1**.

that (a) the synthetic routes used in the present study effectively introduce porphyrin moieties onto the surface of MWCNTs and (b) the peak separation of the C 1s spectrum of MWCNT-based materials can

distinguish between the different carbon species on the surface of porphyrin-functionalized MWCNTs, confirming the success of the tin porphyrin grafting process.

2.8 Nonlinear optical properties

Within the family of carbon nanotubes, MWCNT materials possess the advantages of low cost and high laser damage threshold, and are therefore suitable for high-power laser applications. The NLO properties of MWCNT-SnTPP **1** and MWCNT-SnTPP **2** were initially studied in the ps regime using the open-aperture Z-scan method (for comparative purposes, the open-aperture Z-scan spectra of SnTPP **1**, SnTPP **2**, and the MWCNT/SnTPP **1** and MWCNT/SnTPP **2** blends are also provided (Figs. S3 and S4 in the ESM)), which is a widely used procedure in the evaluation of nonlinear absorption processes; for comparison, pristine MWCNTs were also studied under the same conditions. As shown in Fig. 9, the normalized transmittance increased as the samples were brought closer to the focus, which is contrary to an optical limiting response and indicative of saturable absorption properties. For MWCNTs, the inter-band transition of semiconducting electronic structures plays an important role for the saturation [45]; the electrons in the valence band of the MWCNTs undergo a transition to the conduction band under the action of the laser pulse, and the high intensity of the pulse depletes electrons in the valence band and results in absorbance decrease [46]. The weaker saturable absorption response for the nanohybrids MWCNT-SnTPP **1** and MWCNT-SnTPP **2** compared to that of MWCNTs may be due to the opposing nature of the nonlinear absorption properties of MWCNTs in comparison with the porphyrin units (SnTPP **1** and SnTPP **2**) [8]. Indeed, individual SnTPP **1** and SnTPP **2** are reverse saturable absorbers under the same excited conditions (Fig. S3 in the ESM). Interestingly, no obvious Z-scan signal was detected in the measurement for the blend suspensions as shown in Fig. S4 (in the ESM). This may be ascribed to competition between saturable absorption and reverse saturable absorption, consistent with the results of the mixture of reduced graphene oxide and zinc phthalocyanine in Ref. [47]. Specifically, the saturable absorption behavior of the MWCNTs might be offset by the reverse saturable absorption behavior of the porphyrin moieties and the photo-induced electron/energy transfer between them. Although the saturable absorption performance of the new porphyrin-functionalized MWCNTs is inferior to that of MWCNTs, there are also some advantages. The insoluble nature of MWCNTs makes their molecular properties difficult to study, and limits their use in practical applications. The covalent attachment of porphyrin units is expected to facilitate the development of applications by improving solubility and ease of dispersion, and also by providing options for chemical attachment to surfaces [12]. The nanohybrids of MWCNTs involving covalent functionalization by porphyrins are therefore better candidates than the pristine MWCNTs for applications as saturable absorbers, such as in pulse shaping and shutters in ps systems. Although few studies on the application of MWCNT materials as saturable absorbers under femtosecond conditions have been reported [48], the MWCNT-based materials, such as MWCNT-SnTPP **1** and MWCNT-SnTPP **2**, offer much simpler and cheaper fabrication than conventional semiconductor saturable absorber mirrors, and can be easily integrated into optical-fiber communication systems.

To gain further insight into the nonlinear absorption performance, open-aperture Z-scan measurements were also performed at 532 nm with nanosecond laser pulses; the results are shown in Fig. 10. MWCNTs, SnTPP **1**, SnTPP **2**, MWCNT-SnTPP **1**, MWCNT-SnTPP **2**, and two control samples of MWCNTs with

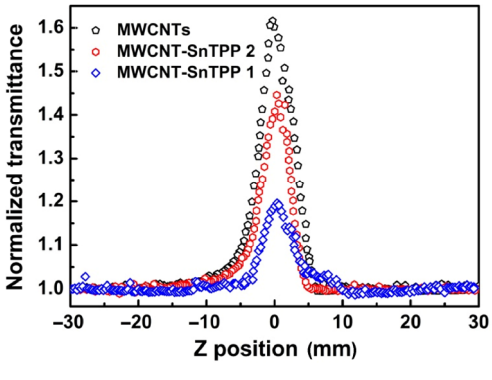

Figure 9 Open-aperture Z-scan curves for pristine MWCNTs, MWCNT-SnTPP **1**, and MWCNT-SnTPP **2** at a wavelength of 532 nm in the ps regime.

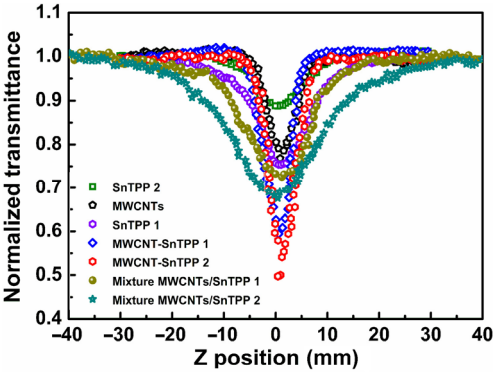

Figure 10 Normalized open-aperture Z-scan data of MWCNTs, SnTPP **1**, SnTPP **2**, MWCNT-SnTPP **1**, MWCNT-SnTPP **2**, blended MWCNTs and SnTPP **1**, and blended MWCNTs and SnTPP **2** at a wavelength of 532 nm in the ns regime.

porphyrins in DMSO were used as references. As the samples were brought closer to the focus, the beam intensity increased, and the nonlinear effect resulted in decreased transmittance. In other words, all of the compounds exhibited significant reverse saturable absorption under the open-aperture configuration corresponding to a positive nonlinear absorption, a property that is applicable in the protection of optical sensors [49]. The third-order NLO absorption response of MWCNT-SnTPP **1** was superior to those of MWCNTs, SnTPP **1**, SnTPP **2**, and the MWCNTs/SnTPP **1** and MWCNTs/SnTPP **2** blends, but inferior to that of MWCNT-SnTPP **2**. These experimental results were consistent with the reports of graphene oxide covalently functionalized by zinc phthalocyanine [7]. This observation clearly indicated that the synthetic approaches and the porphyrin content exert a crucial effect on the third-order nonlinear optical properties of the resultant porphyrin-functionalized MWCNT systems. Both MWCNT-SnTPP nanohybrids exhibited higher nonlinear absorption performance than the C_{60}-porphyrin system in Ref. [50], but further comment is not warranted owing to the use of a different experimental geometry.

Under nanosecond pulse conditions at 532 nm, SnTPP **1** and SnTPP **2** exhibited reverse saturable absorption arising from excited-state absorption, similar to other porphyrin derivatives [50], while MWCNTs showed strong optical limiting effects in the nanosecond regime, which mainly arose from strong nonlinear light scatterings because of the creation of new scattering centers consisting of ionized carbon microplasmas and solvent microbubbles [42]; reverse saturable absorption from the porphyrin moieties and nonlinear scattering from the MWCNTs should therefore each contribute to the increased NLO effect for MWCNT-SnTPP **1** and MWCNT-SnTPP **2**. Similar to graphene and SWCNTs [20, 51], the donor-acceptor interaction between the MWCNTs and porphyrins in the present nanohybrids includes an intermolecular charge transfer from the photo-excited singlet porphyrin to the MWCNTs, resulting in fluorescence quenching and energy release. In the present study, the effective electron/energy transfer was confirmed by detailed Raman and fluorescence spectra of the porphyrin-functionalized MWCNTs. Since photo-induced electron/energy transfer results in a charge-separated state, which leads to large nonlinear absorption, as observed in the poly-(N-vinyl carbazole) (PVK)-modified SWCNT system and SWCNT-porphyrin nanohybrids [19, 52], the photo-induced electron/energy transfer from electron-donor porphyrin to electron-acceptor MWCNTs should be an important contributor to the observed NLO effects. A combination of different nonlinear mechanisms is likely to be responsible for the improved NLO response; however, it is difficult to determine which mechanism is dominant with the MWCNT-SnTPP suspensions.

It should be noted that the behaviors of MWCNT-SnTPP **1** and MWCNT-SnTPP **2** were quite different at the ns and ps time scales. The transition from saturable absorption (ps) to reverse saturable absorption (ns) may be the result of transitions from the first excited state to higher excited states arising from the temporally longer pulse width under ns conditions [53–56]. Both saturable absorption and reverse saturable absorption originate from an excited-state absorption process. With both ns and ps laser pulses, MWCNT-SnTPP nanohybrids were pumped into an excited state. However, in the ns regime with an increased pulse duration and laser intensity, excited-state absorption will play a more important role owing to participation of more excited-state transitions, and so reverse saturable absorption is observed. The MWCNT-SnTPP suspensions exhibited nonlinear absorption with a saturable absorption, which underwent a transition to reverse saturable absorption as the laser intensity and pulse duration increased; this makes MWCNT-SnTPP

materials possible candidates for practical applications as saturable absorbers, optical switches, and mode-locking elements or optical limiters in eye and sensor protection for ns pulses. The work function of the MWCNTs is controlled by the chemical functionalization (and indeed the different synthetic routes), so one can expect such functionalization to lead to the control, tuning, and tailoring of the NLO properties of the MWCNTs. Although more work is needed to determine other potential applications of the novel nanohybrid materials, this approach opens new possibilities for research on the construction of carbon-nanotube-based materials, and it may be extended to hybrids of other nanostructured materials in which agglomeration is not expected.

3 Conclusions

MWCNT nanohybrids covalently functionalized by axially coordinated metal-porphyrins and showing significant reverse saturable absorption with nanosecond pulses and saturable absorption in the picosecond regime have been prepared and characterized through various spectroscopic techniques. The synthetic approach was found to be an important factor influencing the photophysical properties (including NLO performance) of the porphyrin-functionalized MWCNTs. Results showed that nonlinear absorption properties of covalently linked materials are enhanced under nanosecond pulse conditions and originate from a combination of nonlinear mechanisms. The observed saturable absorption and reverse saturable absorption exhibited by the MWCNT-SnTPP nanohybrids suggest that they could be potential candidates for applications in ultrafast optical switching and optical limiting. The present work revealed important insights into the NLO effects of nanohybrids of metal-porphyrins and carbon nanotubes, and can provide new guidelines for the design of carbon-nanotube-based NLO materials.

4 Experimental

4.1 Materials

MWCNTs were provided by Beijing DK Nanotechnology Co. Ltd, China, and were used as received. All reactions were carried out under a nitrogen (N_2) atmosphere with the use of standard Schlenk techniques. All reagents used in this work were chemical or analytical grade, and deionized water was used for all experiments. DMF and pyridine were dried over CaH_2 and distilled before use. Other reagents and chemicals were obtained from commercial suppliers and used without further purification. SnTPP **1** and SnTPP **2** were prepared according to literature procedures [57, 58].

4.2 Characterization

Samples were prepared in the form of KBr pellets, and FTIR spectra were acquired with an MB154S-FTIR spectrometer (Canada) in the range 400–4,000 cm^{-1}. The UV-vis absorption spectra were recorded with a JASCO V-570 spectrophotometer at room temperature in the range 200–800 nm. Fluorescence spectra were recorded with a Fluoro-Max-P fluorescence spectrophotometer. The excitation wavelength was fixed at 420 nm. Raman spectra of the samples were measured on a Renishaw inVia Raman microscope excited at a wavelength of 532 nm. All experiments were carried out at room temperature. TEM studies were performed using a JEM-2100 (JEOL) instrument working at 200 kV. Samples were supported on amorphous carbon-coated copper grids. XPS measurements were conducted on an RBD upgraded PHI-5000C ESCA electron spectrometer (PerkinElmer) with a Mg Kα excitation source at 280 eV to investigate the chemical nature and elemental composition of the samples. TGA was performed using a PerkinElmer Pyris 1 system at a heating rate of 10 ˚C·min^{-1} from 50 to 800 ˚C under a N_2 purge. The weight of each sample was ca. 5 mg.

4.3 Investigation of NLO properties

The nonlinear absorption properties of all samples were measured with linearly polarized 4-ns and 21-ps pulsed 532-nm light generated from a mode-locked Nd:YAG laser with a repetition rate of 2 Hz. Solutions of the samples in DMSO were mounted on a computer-controlled translation stage, and then moved along the *z*-axis of the incident beam. The input energy and the transmitted energy were measured using two energy detectors (Rjp-765 energy probe), which were

linked to an energy meter (Rj-7620 Energy Ratiometer, Laserprobe). All of the measurements were performed at room temperature, and all of the sample concentrations were adjusted to 0.15 mg·mL^{-1}.

4.4 Preparation of nanohybrid MWCNT-SnTPP 1

Scheme 1 illustrates the synthesis of MWCNT-SnTPP **1** via a straightforward 1,3-dipolar cycloaddition of azomethine ylides. In a typical experiment, MWCNTs (50 mg) were sonicated for 30 min in a 100 mL round-bottomed flask in the presence of DMF (50 mL). Sarcosine (200 mg) and SnTPP **1** (20 mg) were added to the suspension, and the mixture was heated at 130 °C under N_2. Further portions of sarcosine (3 × 200 mg every 24 h) and SnTPP **1** (3 × 10 mg every 24 h) were added, and the reaction was stopped after six days. The resultant solution was poured into iced water (150 mL) and then filtered through a funnel. The solid was washed with water, methanol, CH_2Cl_2, and anhydrous diethyl ether to remove unreacted porphyrins and possible byproducts until the filtrate was colorless. The resulting covalently porphyrin-functionalized MWCNT (MWCNT-SnTPP **1**) was dried under vacuum overnight at room temperature.

4.5 Preparation of nanohybrid MWCNT-SnTPP 2

MWCNT-SnTPP **2** was prepared via a stepwise approach that involved a 1,3-dipolar cycloaddition followed by nucleophilic substitution (Scheme 1). The experimental procedure was as follows: MWCNTs (40 mg) were sonicated for 30 min in DMF (50 mL). 4-Hydroxybenzaldehyde (80 mg) was added to the suspension, and the mixture was heated at 130 °C. Sarcosine (800 mg) was added in portions (4 × 200 mg every 24 h), and the reaction was stopped after six days. After this period, 150 mL of deionized water was added to the mixture. Filtration gave the crude product, which was washed with deionized water, methanol, and then ethanol, affording the 4-hydroxybenzaldehyde-functionalized MWCNT hybrid as a black solid that was thoroughly vacuum-dried at room temperature for 24 h. The product thus obtained was used for the subsequent reaction. To a stirred solution of 4-hydroxybenzaldehyde-functionalized MWCNTs (30 mg) in pyridine (40 mL) under a N_2 atmosphere was added SnTPP **2** (100 mg). The resulting mixture was stirred under reflux for four days, and then the crude product was isolated by filtration, and the black solid was washed thoroughly with several portions of deionized water, CH_2Cl_2, methanol, and ethanol, and then dried under vacuum overnight.

Acknowledgements

Financial support from the National Natural Science Foundation of China (Nos. 51432006, 50925207, and 51172100), the Ministry of Science and Technology of China for the International Science Linkages Program (No. 2011DFG52970), the Ministry of Education of China for the Changjiang Innovation Research Team (No. IRT14R23), the Ministry of Education and the State Administration of Foreign Experts Affairs for the 111 Project (No. B13025), 100 Talents Program of CAS, and Jiangsu Innovation Research Team are gratefully acknowledged. M. G. H., M. P. C., and C. Z. thank the Australian Research Council (ARC) for support.

Electronic Supplementary Material: Supplementary material (details of O 1s core-level XPS spectra of MWCNT-SnTPP **1** and MWCNT-SnTPP **2**, the fluorescence spectrum of MWCNTs in DMSO, the open-aperture Z-scan curves of SnTPP **1**, SnTPP **2**, blended MWCNTs and SnTPP **1**, and blended MWCNTs and SnTPP **2**) is available in the online version of this article at http://dx.doi.org/10.1007/s12274-015-0928-2.

References

[1] Jariwala, D.; Sangwan, V. K.; Lauhon, L. J.; Marks, T. J.; Hersam, M. C. Carbon nanomaterials for electronics, optoelectronics, photovoltaics, and sensing. *Chem. Soc. Rev.* **2013**, *42*, 2824–2860.

[2] Bao, Q. L.; Loah, K. P. Graphene photonics, plasmonics, and broadband optoelectronic devices. *ACS Nano* **2012**, *6*, 3677–3694.

[3] El Hamaoui, B.; Zhi, L. J.; Wu, J. S.; Li, J. X.; Lucas, N. T.; Tomović, Ž.; Kolb, U.; Müllen, K. Solid-state pyrolysis of polyphenylene-metal complexes: A facile approach toward carbon nanoparticles. *Adv. Funct. Mater.* **2007**, *17*, 1179–1187.

[4] Guezguez, I.; Ayadi, A.; Ordon, K.; Lliopoulos, K.; Branzea, D. G.; Migalska-Zalas, A.; Makowska-Janusik, M.; El-Ghayoury, A.; Sahraoui, B. Zinc induced a dramatic enhancement of the nonlinear optical properties of an azo-based iminopyridine ligand. *J. Phys. Chem. C* **2014**, *118*, 7545–7553.

[5] Anand, B.; Krishnan, S. R.; Podila, R.; Sai, S. S. S.; Rao, A. M.; Philip, R. The role of defects in the nonlinear optical absorption behavior of carbon and ZnO nanostructures. *Phys. Chem. Chem. Phys.* **2014**, *16*, 8168–8177.

[6] Wang, A. J.; Yu, W.; Fang, Y.; Song, Y. L.; Jia, D.; Long, L. L.; Cifuentes, M. P.; Humphrey, M. G.; Zhang, C. Facile hydrothermal synthesis and optical limiting properties of TiO_2-reduced graphene oxide nanocomposites. *Carbon* **2015**, *89*, 130–141.

[7] Zhu, J. H.; Li, Y. X.; Chen, Y.; Wang, J.; Zhang, B.; Zhang, J. J.; Blau, W. J. Graphene oxide covalently functionalized with zinc phthalocyanine for broadband optical limiting. *Carbon* **2011**, *49*, 1900–1905.

[8] Feng, M.; Zhan, H. B. Facile preparation of transparent and dense CdS-silica gel glass nanocomposites for optical limiting applications. *Nanoscale* **2014**, *6*, 3972–3977.

[9] Wang, A. J.; Long, L. L.; Zhao, W.; Song, Y. L.; Humphrey, M. G.; Cifuentes, M. P.; Wu, X. Z.; Fu, Y. S.; Zhang, D. D.; Li, X. F. et al. Increased optical nonlinearities of graphene nanohybrids covalently functionalized by axially-coordinated porphyrins. *Carbon* **2013**, *53*, 327–338.

[10] Liu, Z. B.; Xu, Y. F.; Zhang, X. Y.; Zhang, X. L.; Chen, Y. S.; Tian, J. G. Porphyrin and fullerene covalently functionalized graphene hybrid materials with large nonlinear optical properties. *J. Phys. Chem. B* **2009**, *113*, 9681–9686.

[11] Mackiewicz, N.; Bark, T.; Cao, B.; Delaire, J. A.; Riehl, D.; Ling, W. L.; Foillard, S.; Doris, E. Fullerene-functionalized carbon nanotubes as improved optical limiting devices. *Carbon* **2011**, *49*, 3998–4003.

[12] Wang, A. J.; Fang, Y.; Yu, W.; Long, L. L.; Song, Y. L.; Zhao, W.; Cifuentes, M. P.; Humphrey, M. G.; Zhang, C. Allyloxyporphyrin-functionalized multiwalled carbon nanotubes: Synthesis by radical polymerization and enhanced optical-limiting properties. *Chem.—Asian J.* **2014**, *9*, 639–648.

[13] Liu, Z. B.; Guo, Z.; Zhang, X. L.; Zheng, J. Y.; Tian, J. G. Increased optical nonlinearities of multi-walled carbon nanotubes covalently functionalized with porphyrin. *Carbon* **2013**, *51*, 419–426.

[14] Rahman, S.; Mirza, S.; Sarkar, A.; Rayfield, G. W. Design and evaluation of carbon nanotube based optical power limiting materials. *J. Nanosci. Nanotechnol.* **2010**, *10*, 4805–4823.

[15] Wang, H.; Hobbie, E. K. Amphiphobic carbon nanotubes as macroemulsion surfactants. *Langmuir* **2003**, *19*, 3091–3093.

[16] Wang, A. J.; Fang, Y.; Long, L. L.; Song, Y. L.; Yu, W.; Zhao, W.; Cifuentes, M. P.; Humphrey, M. G.; Zhang, C. Facile synthesis and enhanced nonlinear optical properties of porphyrin-functionalized multi-walled carbon nanotubes. *Chem.—Eur. J.* **2013**, *19*, 14159–14170.

[17] Mackiewicz, N.; Delaire, J. A.; Rutherford, A. W.; Doris, E.; Mioskowski, C. Carbon nanotube-acridine nanohybrids: Spectroscopic characterization of photoinduced electron transfer. *Chem.—Eur. J.* **2009**, *15*, 3882–3888.

[18] Merhi, A.; Drouet, S.; Kerisit, N.; Paul-Roth, C. O. A family of fluorenyl dendrons for porphyrin dendrimers synthesis. *Tetrahedron* **2012**, *68*, 7901–7910.

[19] Liu, Z. B.; Tian, J. G.; Guo, Z.; Ren, D. M.; Du, F.; Zheng, J. Y.; Chen, Y. S. Enhanced optical limiting effects in porphyrin-covalently functionalized single-walled carbon nanotubes. *Adv. Mater.* **2008**, *20*, 511–515.

[20] Baskaran, D.; Mays, J. W.; Zhang, X. P.; Bratcher, M. S. Carbon nanotubes with covalently linked porphyrin antennae: Photoinduced electron transfer. *J. Am. Chem. Soc.* **2005**, *127*, 6916–6917.

[21] Tagmatarchis, N.; Prato, M. Functionalization of carbon nanotubes via 1,3-dipolar cycloadditions. *J. Mater. Chem.* **2004**, *14*, 437–439.

[22] Tu, W. W.; Lei, J. P.; Jian, G. Q.; Hu, Z.; Ju, H. X. Noncovalent assembly of picket-fence porphyrins on nitrogen-doped carbon nanotubes for highly efficient catalysis and biosensing. *Chem.—Eur. J.* **2010**, *16*, 4120–4126.

[23] Tasis, D.; Tagmatarchis, N.; Bianco, A.; Prato, M. Chemistry of carbon nanotubes. *Chem. Rev.* **2006**, *106*, 1105–1136.

[24] Ballesteros, B.; de la Torre, G.; Ehli, C.; Rahman, G. M. A.; Agulló-Rueda, F.; Guldi, D. M.; Torres, T. Single-wall carbon nanotubes bearing covalently linked phthalocyanines-photoinduced electron transfer. *J. Am. Chem. Soc.* **2007**, *129*, 5061–5068.

[25] Georgakilas, V.; Kordatos, K.; Prato, M.; Guldi, D. M.; Holzinger, M.; Hirsch, A. Organic functionalization of carbon nanotubes. *J. Am. Chem. Soc.* **2002**, *124*, 760–761.

[26] Yang, D. Q.; Rochette, J. F.; Sacher, E. Functionalization of multiwalled carbon nanotubes by mild aqueous sonication. *J. Phys. Chem. B* **2005**, *109*, 7788–7794.

[27] Branca, C.; Frusteri, F.; Magazù, V.; Mangione, A. Characterization of carbon nanotubes by TEM and infrared spectroscopy. *J. Phys. Chem. B* **2004**, *108*, 3469–3473.

[28] Guldi, D. M.; Taieb, H.; Rahman, G. M. A.; Tagmatarchis, N.; Prato, M. Novel photoactive single-walled carbon nanotube-porphyrin polymer wraps: Efficient and long-lived intracomplex charge separation. *Adv. Mater.* **2005**, *17*, 871–875.

[29] Gupta, J.; Vijayan, C.; Maurya, S. K.; Goswami, D. Ultrafast nonlinear optical response of carbon nanotubes functionalized with water soluble porphyrin. *Opt. Commun.* **2012**, *285*, 1920–1924.

[30] Umeyama, T.; Mihara, J.; Tezuka, N.; Matano, Y.; Stranius, K.; Chukharev, V.; Tkachenko, N. V.; Lemmetyinen, H.; Noda, K.; Matsushige, K. et al. Preparation and photophysical and photoelectrochemical properties of a covalently fixed porphyrin-chemically converted graphene composite. *Chem.—Eur. J.* **2012**, *18*, 4250–4257.

[31] Sugiura, K.; Kato, A.; Lwasaki, K.; Miyasaka, H.; Yamashita, M.; Hino, S.; Arnold, D. P. Unusual regioselective mercuration of metalloporphyrins and its potential applications. *Chem. Commun.* **2007**, 2046–2047.

[32] Wojcik, A.; Kamat, P. V. Reduced graphene oxide and porphyrin. An interactive affair in 2-D. *ACS Nano* **2010**, *4*, 6697–6706.

[33] Bottari, G.; de la Torre, G.; Guldi, D. M.; Torres, T. Covalent and noncovalent phthalocyanine-carbon nanostructure systems: Synthesis, photoinduced electron transfer, and application to molecular photovoltaics. *Chem. Rev.* **2010**, *110*, 6768–6816.

[34] Yang, S. Y.; Ma, C. C. M.; Teng, C. C.; Huang, Y. W.; Liao, S. H.; Huang, Y. L.; Tien, H. W.; Lee, T. M.; Chiou, K. C. Effect of functionalized carbon nanotubes on the thermal conductivity of epoxy composites. *Carbon* **2010**, *48*, 592–603.

[35] Zhu, M. S.; Li, Z.; Xiao, B.; Lu, Y. T.; Du, Y. K.; Yang, P.; Wang, X. M. Surfactant assistance in improvement of photocatalytic hydrogen production with the porphyrin noncovalently functionalized graphene nanocomposite. *ACS Appl. Mater. Interfaces* **2013**, *5*, 1732–1740.

[36] Rao, A. M.; Eklund, P. C.; Bandow, S.; Thess, A.; Smalley, R. E. Evidence for charge transfer in doped carbon nanotube bundles from Raman scattering. *Nature* **1997**, *388*, 257–259.

[37] Lim, S. H.; Elim, H. I.; Gao, X. Y.; Wee, A. T. S.; Ji, W.; Lee, J. Y.; Lin, J. Electronic and optical properties of nitrogen-doped multiwalled carbon nanotubes. *Phys. Rev. B* **2006**, *73*, 045402.

[38] Dresselhaus, M. S.; Jorio, A.; Saito, R. Characterizing graphene, graphite, and carbon nanotubes by Raman spectroscopy. *Ann. Rev. Condensed Matter Phys.* **2010**, *1*, 89–108.

[39] Bahr, J. L.; Yang, J. P.; Kosynkin, D. V.; Bronikowski, M. J.; Smalley, R. E.; Tour, J. M. Functionalization of carbon nanotubes by electrochemical reduction of aryl diazonium salts: A bucky paper electrode. *J. Am. Chem. Soc.* **2001**, *123*, 6536–6542.

[40] Zhuang, Q. X.; Mao, X. Y.; Xie, Z.; Liu, X. Y.; Wang, Q.; Chen, Y.; Han, Z. W. Synthesis of multiwalled carbon nanotube/fluorine-containing poly(p-phenylene benzoxazole) composites exhibiting greatly enhanced dielectric constants. *J. Polym. Sci., Part A: Polym. Chem.* **2012**, *50*, 4732–4739.

[41] Ehli, C.; Rahman, G. M. A.; Jux, N.; Balbinot, D.; Guldi, D. M.; Paolucci, F.; Marcaccio, M.; Paolucci, D.; Melle-Franco, M.; Zerbetto, F. et al. Interactions in single wall carbon nanotubes/pyrene/porphyrin nanohybrids. *J. Am. Chem. Soc.* **2006**, *128*, 11222–11231.

[42] Zheng, C.; Feng, M.; Du, Y. H.; Zhan, H. B. Synthesis and third-order nonlinear optical properties of a multiwalled carbon nanotube-organically modified silicate nanohybrid gel glass. *Carbon* **2009**, *47*, 2889–2897.

[43] Yang, K.; Gu, M. Y.; Guo, Y. P.; Pan, X. F.; Mu, G. H. Effects of carbon nanotube functionalization on the mechanical and thermal properties of epoxy composites. *Carbon* **2009**, *47*, 1723–1737.

[44] Zhang, G. X.; Sun, S. H.; Yang, D. Q.; Dodelet, J. P.; Sacher, E. The surface analytical characterization of carbon fibers functionalized by H_2SO_4/HNO_3 treatment. *Carbon* **2008**, *46*, 196–205.

[45] Lauret, J. S.; Voisin, C.; Cassabois, G.; Delalande, C.; Roussignol, P.; Jost, O.; Capes, L. Ultrafast carrier dynamics in single-wall carbon nanotubes. *Phys. Rev. Lett.* **2003**, *90*, 057404.

[46] Zhang, X. L.; Liu, Z. B.; Zhao, X.; Yan, X. Q.; Li, X. C.; Tian, J. G. Optical limiting effect and ultrafast saturable absorption in a solid PMMA composite containing porphyrin-covalently functionalized multi-walled carbon nanotubes. *Opt. Express* **2013**, *21*, 25277–25284.

[47] Zhao, X.; Yan, X. Q.; Ma, Q.; Yao, J.; Zhang, X. L.; Liu, Z. B.; Tian, J. G. Nonlinear optical and optical limiting properties of graphene hybrids covalently functionalized by phthalocyanine. *Chem. Phys. Lett.* **2013**, *577*, 62–67.

[48] Avouris, P.; Freitag, M.; Perebeions, V. Carbon-nanotube photonics and optoelectronics. *Nat. Photonics* **2008**, *2*, 341–350.

[49] Wang, A. J.; Yu, W.; Xiao, Z. G.; Song, Y. L.; Long, L. L.; Cifuentes, M. P.; Humphrey, M. G.; Zhang, C. A 1,3-dipolar cycloaddition protocol to porphyrin-functionalized reduced graphene oxide with a push-pull motif. *Nano Res.* **2015**, *8*, 870–886.

[50] Filidou, V.; Chatzikyriakos, G.; Iliopoulos, K.; Couris, S.; Bonifazi, D. The effect of charge transfer on the NLO response of some porphyrin-[60]fullerene dyads. *AIP Conf. Proc.* **2010**, *1288*, 188–191.

[51] Jahan, M.; Bao, Q. L.; Loh, K. P. Electrocatalytically active graphene-porphyrin MOF composite for oxygen reduction reaction. *J. Am. Chem. Soc.* **2012**, *134*, 6707–6713.

[52] Wu, W.; Zhang, S.; Li, Y.; Li, J. X.; Liu, L. Q.; Qin, Y. J.; Guo, Z. X.; Dai, L. M.; Ye, C.; Zhu, D. B. PVK-modified single-walled carbon nanotubes with effective photoinduced

electron transfer. Macromolecules. *Macromolecules* **2003**, *36*, 6286–6288.

[53] Gurudas, U.; Brooks, E.; Bubb, D. M.; Heiroth, S.; Lippert, T.; Wokaun, A. Saturable and reverse saturable absorption in silver nanodots at 532 nm using picosecond laser pulses. *J. Appl. Phys.* **2008**, *104*, 073107.

[54] Luo, S. L.; Liu, X. E.; Wu, D. Q.; Shi, G.; Mei, T. Tunable conversion from saturable absorption to reverse saturable absorption in poly(pyrrole methine) derivatives. *J. Mater. Chem. C* **2014**, *2*, 8850–8853.

[55] Gao, Y. C.; Chang, Q.; Ye, H. G.; Jiao, W.; Song, Y. L.; Wang, Y. X.; Qin, J. Saturable and reverse saturable absorption of a linear polymer in dimethylformamide. *Appl. Phys. B* **2007**, *88*, 255–258.

[56] Dini, D.; Vagin, S.; Hanack, M.; Amendola, V.; Meneghetti, M. Nonlinear optical effects related to saturable and reverse saturable absorption by subphthalocyanines at 532 nm. *Chem. Commun.* **2005**, 3796–3798.

[57] Crossley, M. J.; Thordarson, P.; Wu, R. A.-S. Efficient formation of lipophilic dihydroxotin(IV) porphyrins and bis-porphyrins. *J. Chem. Soc., Perkin Trans.* **2001**, *1*, 2294–2302.

[58] Lazarides, T.; Kuhri, S.; Charalambidis, G.; Panda, M. K.; Guldi, D. M.; Coutsolelos, A. G. Electron vs energy transfer in arrays featuring two bodipy chromophores axially bound to a Sn(IV) porphyrin via a phenolate or benzoate bridge. *Inorg. Chem.* **2012**, *51*, 4193–4204.